THE SPECIFIC ENERGY ABSORPTION OF LOCAL WOOD SUBJECTED TO QUASI-STATIC LOADING

PROFESOR DR. MD RADZAI BIN SAID
MOHD FIRDAUS BIN ZAKARIA
MOHD KHAIRIR BIN ISMAIL

UNIVERSITI TEKNIKAL MALAYSIA MELAKA

THE SPECIFIC ENERGY ABSORPTION OF LOCAL WOOD SUBJECTED TO QUASI-STATIC LOADING

[1]Md. Radzai Bin Said, [2]Mohd Firdaus B Zakaria and [2]Mohd Khairir Bin Ismail

Fakulti Kejuruteraan Mekanikal, Universiti Teknikal Malaysia Melaka, Melaka

e-mail: [1]radzai@utem.edu.my, [2]messimestup@yahoo.com.my, [2]khairir.ismail@gmail.com

Abstract

An experimental investigation was carried out to study the specific energy absorbed of malaysia local wood. Eleven species of wood were chosen which are, Nyatoh (Palaquim Obovatum), Merbau (Intsia Bijuga), Meranti Putih (Shorea Macroptera), Kelapa Sawit (Elais Guineensis), Kempas (Koompasia Malaccensis), Jati (Tectona Grandis), Cengal (Neobalanocarpus Heimii), Meranti Merah (Shorea Collina), Balau Cina (Shorea spp.), Balau Merah (Shorea spp.), and Kapur (Dryobalanops Aromatia). The experiment was performed in quasi-statically compression method using universal testing machine to obtain the material mechanical properties. Specimens were loaded in axial, circumferential and radial directions. Kink-band phenomena was observed and studied. The deformation mode and the load-displacement curve for axial, circumferential and radial compression of local woods, the highest value of energy absorption and kink-band phenomena as well as its effect on energy absorption were determined and discussed in this paper.

Keywords: cellular materials, local wood, kink band, specific energy absorption

1.0 Introduction

1.1 Wood

Wood has historically been, and indeed remains today as one of the most widely used structural materials. It is a naturally occurring, renewable, biodegradable and relatively low-cost material with outstanding axial stiffness-to-weight and strength-to-weight ratios [1].

There are varieties of wood in Malaysia. From all types of wood, palm oil tree has the most number compared to others. Based on report from Malaysia Palm Oil Berhad (MPOB), palm oil estates consist of 3.6 million hectares and produce 35 million tons of biomass every year. Thus, this type of waste can be reuse as impact energy absorption device, and hence reduces the metallic material consumption as well as preserves the environment. This is feasible since, wood has a unique characteristic in its three principal directions. Its axial compressive strength is much higher than that of radial and circumferential direction. More energy can be absorbed in axial direction.

During axial compression, kinking happens at three stages. Kinking failure is the compression strength limiting mechanism in many advanced composite materials as well as in wood [2-8]. Moran et al. [6] identified three distinct stages of kinking in carbon fiber composites: incipient kinking, transient kinking and steady-state kinking. In this study, it is found that these three stages also govern compressive kinking in wood. Incipient kinking begins shortly before the peak stress and causes the initially linear stress-displacement curve to become non-linear, as illustrated in Fig. 1. The non-linearity is the cumulative effect of many localized regions of incipient kinking. Incipient kinking occurs on a very small scale and initiates near resin canals which are scattered throughout the material. The resin canals cause small areas of fibers to be highly misaligned. The softest deformation mode in this type of microstructure is a localized plastic shearing and buckling of the fibers, and it is also known as incipient kinking. During this process the applied stress continues to rise until the peak stress is attained. The peak stress marks the end of incipient kinking. The incipient kinking stage is followed by the transient stage during which the localized areas of incipient kinking grow and coalesce thus forming a single dominant kink band across the specimen (denoted by point (b) in Fig. 1). During this process the stress drops from its peak value to a steady-state value. Within the dominant band the fibers undergo a complex mode of deformation involving both axial compression and rotation. Eventually, however, volumetric lock-up stiffens the response of the fibers within the kink band and further rotation and axial compression is no longer represents the softest mode of deformation. This marks the end of transient kinking. At this stage the easiest mode of deformation is for the kink band to broaden laterally into the surrounding material. This occurs under a constant applied stress and is called steady-state band broadening, as shown in Fig. 1. It is important to realize that no further deformation of the fibers within the kink band occurs during band broadening. Instead, the fibers at the edges of the kink band are rotated and axially compressed thus broadening the

band. In this paper the mechanisms governing kinking in wood within the context of the three stages described above are discussed. Comparison is made with the mechanisms governing kinking in carbon fiber composites as reported by Moran et al. [6].

The different characteristic, failure mode and the ability of local wood to absorb impact energy are also discussed in conjunction with the quasi-static data obtained in the experiment.

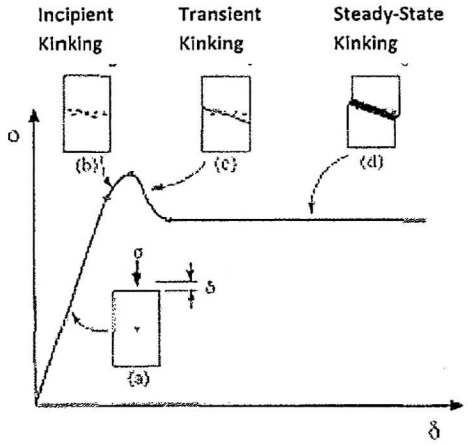

Figure 1: Overall stress-end shortening behavior of kinking in spruce compressed in the fiber direction. (a) Linear elastic loading. (b) Incipient kinking under increasing load. (c)Transient kinking under decreasing load. (d) Steady-state kinking under constant load. [6]

2.0 Experimental Developments

2.1 Specimens

Experiments were performed on local wood specimens over a wide range of densities between 171 and 967 kg/m^3. Square specimens were machined from large blocks of local wood and the surfaces was polished using 320 grit sand papers. The specimen dimensions were typically 40mm x 40mm x 40mm.

2.2 Experimental Method

The specimen was compressed by an axial quasi-static load using a 200kN universal testing machine (UTM) at a loading rate of 5 mm/min. The load displacement curves in the tests were obtained from the computer attached to the UTM machine using Bluehill software. The data then were transferred to Sigmaplot to calculate the energy at locking.

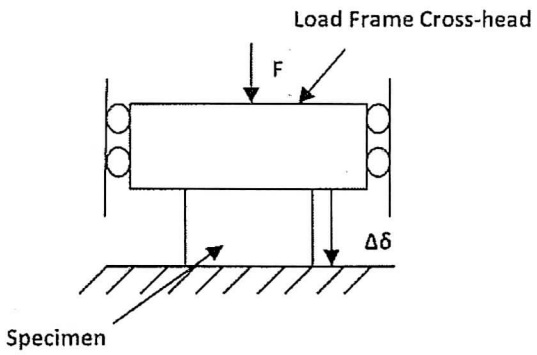

Figure 2: Schematic of the quasi-static test setup.

3.0 Results and Discussion

Figure 3 to Figure 5 shows the load-displacement curves for selected specimen determined from the compression tests. The force at locking F_L, locking displacement δ_L , and energy at locking were obtained using Sigmaplot by calculating the area below the curve for each graph. To determine the force at locking and the locking displacement, a straight-line approximation for the curve was done using linear regression approximation and another straight line was made perpendicular to the initial portion of the load-displacement curve which is shown by the straight line with a steep slope in the graph. The point where this two straight lines met is the locking point and used as a reference point to determine the force at locking and the locking displacement. The absorbed energy was obtained by calculating the area under the curve until the locking point. From the graph, it can be seen that the force at locking for compression at axial direction is larger than that of compression at circumferential and radial direction. Kempas shows the largest reading of force at locking for compression at axial direction as hown in Table 1 in Appendix 1.

On the other hand, the amount for energy per mass varies according to compression direction. Compression at axial direction shows the largest amount of energy absorbed by specimens compared to radial and circumferential direction. The amount of energy absorbed depends on the value of stress and strain at locking. Kempas has the largest average energy absorption value compared to other specimen. During the compression test, high resolution video camera was used to capture the image of the specimen transformation from start to the end.

Figure 3 shows the transformation of Meranti Putih during compression in axial direction. The numbers (1) – (10) on the curve refer to the specimen change pictures captured at these points. At point (3)

the specimen reached its yield stress as well as the incipient kinking stage. There is sign of collapse where the fibers have severely misaligned and maximum shear occurred from 10^0 to 45^0 angles. Poulsen and Tonnesen [8] measured the kink band angle in spruce to be approximately 23°. The curve starts to show non-linearity as the most severely misaligned fibers begin to shear plastically and buckle. After point (3), the stress drops steadily (as in figure 3) as it enters transient kinking stage. During this process, the fibers within the dominant kink band continue to rotate and compress axially while the deformation within the other kink band was halted. The applied stress continued to drop. After the fibers within the dominant kink band have rotated 60° from their initial orientation, and have been axially compressed by about 50%, lockup phenomenon has occurred. At this stage the dominant kink band is about 5 fiber diameters wide. After this point; the specimen has reached steady state kinking stage that marked the end of transient kink stage. This phenomenon continues along the plastic zone as can be seen from Figure 3 point (6) – (10). The constant applied stress needed to broaden the kink band is known as the steady-state band broadening stress [6]. After point (10), the specimen reaches densification stage. Continued compression results in the compaction of deformed and ruptured cell walls against each other, leading to rapid increase in crushing stress since internal voids are almost eliminated.

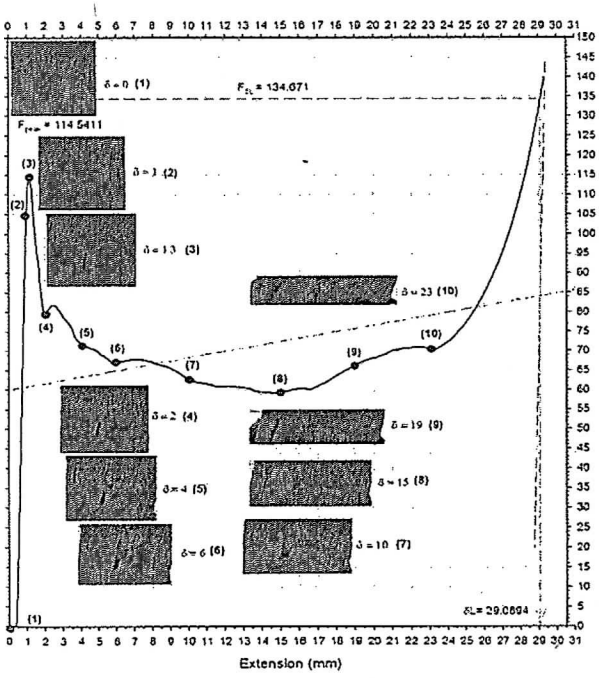

Figure 3: Compression Test for Meranti Putih MP3A (axial direction)

The change mode for circumferential and radial direction differs from axial direction compression. Figure 4 shows the changing stages of Meranti Putih for circumferential compression. At point (2), the specimen reached its yield stress and at the edge of elastic point. After this point, the specimen entered the plastic region. Compared with axial direction, circumferential and radial direction compression does not show kink band phenomena but on the other hand, shear band has occurred. This is why a smoother curve was obtained due to the cells collapse in uniform manner. The yield stress is also 1/5 lower than that of axial direction. At point (13) it reaches densification stage. Some of the materials are not suitable to use as IEA device in circumferential and radial direction as they react in brittle manner when subjected to force. The examples for this case are, Jati, Balau Cina and Balau Merah.

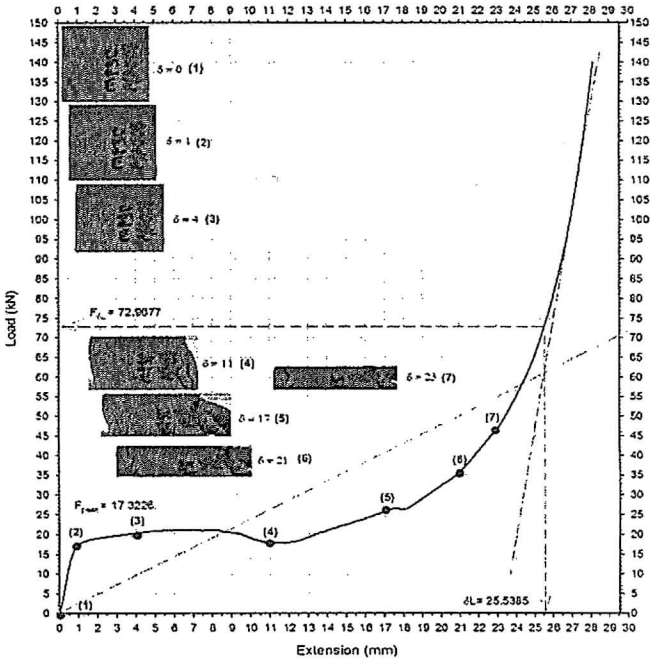

Figure 4: Compression Test for Meranti Putih MP3C (circumferential direction)

From the experiments that have been done, it is found that Kempas has the best average energy absorption in axial direction compression which is **41.507kJ/kg.** Jati, Balau Merah and Balau Cina are not suitable to be used as IEA device in radial and circumferential direction as they tend to rupture under compressive load, leading to a sudden drop of

energy. The ability to absorb energy does not always depend on the specimen density for local wood as shown in the experiment.

Reference

[1] Andre Da Silva, Stelios Kyriakides “ Compressive Response and Failure of Balsa Wood. Journal of Solids and Structures 44 (2007). 8685-8717(2007).

[2] Fleck, N.A., P.M. Jelf and P.M. Curtis, “ Compressive failure of laminated and woven composites, J. Compos. Tech. Res.17,212-220 (1995).

[3] Floyd P. Henry, “A Comparison of Requirements and Test Methodologies for a Variety of Impact Absorbing Materials. General Plastics Mfg. Co. International Symposium, Chicago, il USA.(2001).

[4] J.S. Poulsen , P.M. Moran , C.F.Shih, E.Byskov . “ Kink Band Initiation and Band Broadening in Clear Wood under Compressive Loading. Mechanics of Materials 25(1997)67-77 (1997).

[5] Kucera, L.J. and M. Bariska “ On the fracture morphology in wood, Part 1, Wood Sci. Technol. 16,241-259 (1982).

[6] Moran, P., X.H. and C.F.Shih, “ Kink band formation and band broadening in fiber composites under compressive loading, Acta Met. Mater. 43, 2943-2958 (1995).

[7] M. Vural , G. Ravichandran , “ Dynamic Response and Energy Dissipation Characteristics of Balsa Wood: experiment and analysis Journal of Solids and Structures 40(2003) 2147-2170 (2007).

[8] Poulsen, J.S., M. Tonnesen and E. Byskov, “ Strain Localization in Clear Wood in Compression, in: Computational Mechanics '95, Proceedings of International Confrence on Computational Engineering Science, Hawaii, USA, pp.1785-1790 (1995).

[9] S.S. Cheon and S.A. Meguid , “ Crush Behavior of Metallic Foams for Passenger Car Design. Journal of Automotive Technology.Vol 5,N0 1, 47-53 (2004).

[10] S.R.Reid and C.Peng. “ Dynamic Uniaxial Crushing of Wood. I.t. J. Impact Engng, Vol. 19, Nos. 5-6, pp.531-570 (1997).

[11] Timothy J. Van Pelt. “ Biomass Densification. Agricultural Engineering 537.Iowa State University
(2002).

APPENDIX 1

Table 1: Result of the quasi-static compression of wood specimens (axial, circumferential and radial directions)

Wood (specimen)	F_{peak} (kN)	Density (kg/m^3)	$\Delta\delta_L$(mm)	$F_{\delta L}$ (kN)	$E_{\delta L}$ (kJ)	E_{Yield} (kJ)	E_S (kJ/kg)
Kempas (axial)	87.545	726.876	28.182	128.797	1.937	0.128	41.507
Kempas (circumferential)	19.742	745.365	26.134	88.89	0.774	0.009	16.211
Kempas (radial)	18.936	747.448	26.478	81.974	0.769	0.009	16.081
Meranti Putih (axial)	113.279	732.396	29.364	128.749	1.839	0.047	39.069
Meranti Putih (circumferential)	17.123	715.781	26.277	70.749	0.82	0.01	17.883
Meranti Putih (radial)	15.773	733.646	25.851	86.948	0.871	0.011	18.508
Merbau (axial)	95.585	781.875	31.915	125.456	2.038	0.051	40.715
Merbau (circumferential)	18.136	711.25	27.445	72.562	0.754	0.008	15.553
Merbau (radial)	16.317	783.047	28.675	83.952	0.798	0.007	15.905
Jati (axial)	101.609	754.042	32.9	110.058	1.755	0.064	36.827
Jati (circumferential)	19.536	716.198	27.74	63.419	0.449	0.012	9.831
Jati (radial)	16.339	745.208	29.097	62.819	0.417	0.0073	8.678
Balau Cina (axial)	111.027	835.001	33.384	105.01	1.372	0.069	25.698
Balau Cina (circumferential)	23.303	857.344	28.63	64.774	0.471	0.013	8.587
Balau Cina (radial)	20.877	849.219	29.366	69.732	0.507	0.011	9.325
Balau Merah (axial)	110.025	748.75	34.1	99.784	1.309	0.05	27.305
Balau Merah (circumferential)	11.712	779.427	28.302	41.987	0.268	0.008	5.338
Balau Merah (radial)	12.942	783.542	30.033	46.355	0.296	0.006	5.9
Nyatoh (axial)							

Nyatoh (circumferential)	89.521	730.157	27.925	123.676	1.789	0.05	38.317
Nyatoh (radial)	8.042	708.125	26.143	80.226	0.682	0.003	15.044
Kelapa Sawit (axial)	14.625	727.604	25.694	74.574	0.825	0.007	17.728
Kelapa Sawit (circumferential)	5.6054	190.313	36.198	64.09	0.215	0.008	17.629
Kelapa Sawit (radial)	0.8645	178.4375	27.125	4.955	0.064	0.0005	5.583
	0.8258	185.7813	26.9884	5.058	0.064	0.0006	5.406

Wood (specimen)	F_{peak} *(kN)*	**Density (kg/m^3)**	$\Delta\delta_L$*(mm)*	$F_{\delta L}$ *(kN)*	$E_{\delta L}$ *(kJ)*	E_{yield} *(kJ)*	E_S *(kJ/kg)*
Meranti Merah (axial)	83.978	651.406	30.297	119.994	1.767	0.0455	42.4184
Meranti Merah (circumferential)	11.915	644.375	27.943	53.392	0.57	0.005	13.8514
Meranti Merah (radial)	12.261	635.9375	27.834	56.346	0.496	0.005	13.4787
Kapur (axial)	116.852	758.646	29.529	120.743	1.912	0.052	39.353
Kapur (circumferential)	13.026	732.813	27.212	49.781	0.511	0.006	10.891
Kapur (radial)	17.052	732.813	26.619	51.2645	0.641	0.007	13.143
Cengal (axial)	112.128	874.948	32.264	126.746	1.929	0.075	35.609
Cengal (circumferential)	25.729	841.953	28.455	60.949	0.580	0.021	10.825
Cengal (radial)	26.952	879.948	28.415	63.331	0.539	0.019	9.573